Ultrafast Temporal SU(1,1) Interferometer

Sara Meir, Yuval Tamir, Hamootal Duadi, Eliahu Cohen, and Moti Fridman*
Faculty of Engineering and the Institute of Nanotechnology and Advanced Materials, Bar-Ilan University, Ramat Gan 5290002, Israel

(Received 19 October 2022; accepted 22 May 2023; published 22 June 2023)

Interferometers are highly sensitive to phase differences and are utilized in numerous schemes. Of special interest is the quantum SU(1,1) interferometer which is able to improve the sensitivity of classical interferometers. We theoretically develop and experimentally demonstrate a *temporal* SU(1,1) *interferometer* based on two time lenses in a $4f$ configuration. This temporal SU(1,1) interferometer has a high temporal resolution, imposes interference on both time and spectral domains, and is sensitive to the phase derivative which is important for detecting ultrafast phase changes. Therefore, this interferometer can be utilized for temporal mode encoding, imaging, and studying the ultrafast temporal structure of quantum light.

DOI: 10.1103/PhysRevLett.130.253601

Classical interferometers can detect small phase differences accumulated along their arms and are utilized in different schemes [1,2]. Classical interferometers based on beam splitters have phase sensitivity of $1/\sqrt{N}$, where N is the number of photons, and denoted as SU(2) interferometers [3]. Replacing the beam splitters with parametric amplifiers improves the phase sensitivity to $1/N$, and such interferometers are denoted as SU(1,1) interferometers [3–8]. The estimation of relative phase with such interferometers is utilized in various quantum sensors [9].

Temporal optics rises from the equivalence between the diffraction of light in free space and the dispersion of pulses in dispersive media. Specifically, time lenses impose a quadratic phase in time and can image signals in time or induce Fourier transform on input signals [10–17]. Our time lenses impose the quadratic phase shift via a four-wave mixing (FWM) process between the input signal and a chirped pump [18,19]. The output of the time lens is the amplified signal together with the generated idler resulting from the interaction between the signal and the pump waves. During the process, two pump photons convert into a pair of photons, one in the signal and one in the idler beams.

We extended the SU(1,1) interferometer into the time domain by converting the parametric amplifiers into time lenses [6–8]. We tuned the time lens to perform Fourier transform by setting the image and object planes at focal distances from the time lenses, so each parametric amplifier becomes a temporal $2f$ system. Our temporal SU(1,1) interferometer has the known benefits of improved sensitivity beyond the shot-noise limit. In addition, it has a higher temporal resolution (thanks to the time magnification of the time lenses), it imposes interference on time and spectral domains simultaneously (thanks to the Fourier transform of each $2f$ system), and it is sensitive to the phase derivative as a function of time. This is important because phase estimation composes a major part of analyzing and mapping images and states. This temporal SU(1,1) interferometer can be utilized for quantum imaging of ultrafast signals [20–22], temporal mode encoding [23], and studying the temporal structure of entangled photons [24]. Here, we analyze theoretically and experimentally this temporal SU(1,1) interferometer and investigate the temporal and spectral structure of the input signal.

The temporal SU(1,1) interferometer has two time lenses in a $4f$ configuration leading to interference in the temporal and spectral domains and is schematically shown in Fig. 1. Each time lens has a dispersion of $2D$, D, and $-D$ on the pump, signal, and idler beams, respectively [25,26]. We impose these dispersion values by tuning the types and lengths of fibers in the system. The temporal intensity distribution of the idler is proportional to the Fourier transform of the input signal [25–27]. Since the signal is

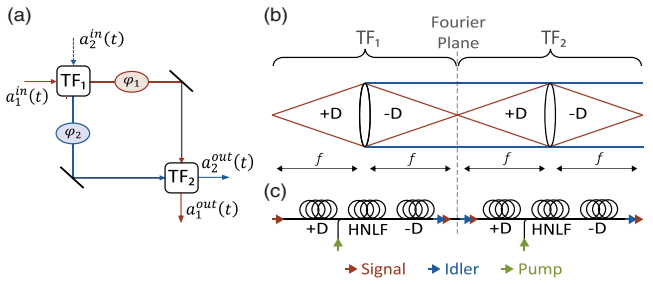

FIG. 1. (a) Schematic of the temporal SU(1,1) interferometer. The two time lenses serve as the beam splitters where each time lens imposes a temporal Fourier transform (TF) on its inputs. (b) Presenting the same interferometer as a temporal $4f$ system with two temporal Fourier transform systems (TF_1 and TF_2). (c) Schematic of the experimental configuration corresponding to the temporal $4f$ system. Red, blue, and green lines or arrows, denote the signal, idler, and pump, respectively.

not affected by the lens, and only by the positive and negative dispersion which cancel each other, it leads to perfect imaging of the signal. So the output signal field is proportional to the input [28,29].

A temporal ray scheme is a convenient way to describe temporal schemes. It is similar to a regular spatial ray scheme after replacing the y axis with a proper time axis [14,30]. In this temporal ray scheme, different wavelengths are denoted by rays at different angles due to dispersion. The temporal ray scheme of our interferometer is shown in Fig. 1(b) and presents the two time lenses in a $4f$ configuration. We also present a simplified scheme of the experimental setup in Fig. 1(c), showing the different components of the system. The dispersion is achieved by optical fibers, and the time lenses are realized by a nonlinear interaction between the chirped pump and the signal and idler modes in a highly nonlinear fiber (HNLF). A detailed schematic of the experimental setup is shown in the Supplemental Material [31].

Each time lens serves as a parametric amplifier with one arm amplifying the input and the other generating the Fourier transform of the input. The input signal and idler fields are denoted as $a_1^{\mathrm{in}}(t)$ and $a_2^{\mathrm{in}}(t)$, so the outputs of the first time lens are

$$a_{1,2} = G_1 a_{1,2}^{\mathrm{in}} + g_1 \mathcal{F}\{a_{2,1}^{\mathrm{in}\dagger}\}, \tag{1}$$

where $G_1 = \cosh(r)$, and $g_1 = \sinh(r)$ are the amplification of the signal and the idler, respectively. The parameter r is proportional to the effective nonlinearity of the time lens and to the pump power.

At the Fourier plane, we induce phases on the signal and the idler, denoted as φ_1 and φ_2, and send them to a second time lens. We assume a strong coherent input only at the signal arm, $a_1^{\mathrm{in}}(t) = \alpha(t)$, and derive the output intensities from the interferometer, as

$$\begin{aligned} I_1^{\mathrm{out}} &= a_1^{\mathrm{out}\dagger} a_1^{\mathrm{out}} \\ &= |\alpha(t)|^2 (G_1^2 G_2^2 + g_1^2 g_2^2 \\ &\quad + 2G_1 G_2 g_1 g_2 \cos(\varphi_1 + \varphi_2)), \end{aligned} \tag{2}$$

$$\begin{aligned} I_2^{\mathrm{out}} &= a_2^{\mathrm{out}\dagger} a_2^{\mathrm{out}} \\ &= |\mathcal{F}\{\alpha^\dagger(t)\}|^2 (g_1^2 G_2^2 + G_1^2 g_2^2 \\ &\quad + 2G_1 G_2 g_1 g_2 \cos(\varphi_1 + \varphi_2)), \end{aligned} \tag{3}$$

where G_2 and g_2 are the amplification parameters of the second time lens. Therefore, the outputs of the interferometer in one arm are the input signal multiplied by $\cos(\varphi_1 + \varphi_2)$, and on the other arm are the Fourier transform of the input multiplied by $\cos(\varphi_1 + \varphi_2)$. Note that although I_2^{out} is proportional to the Fourier transform of $\alpha(t)$ squared, it is still a function of time; the spectrum of $\alpha(t)$ is mapped to $I_2^{\mathrm{out}}(t)$.

We add a high dispersion fiber at the output (shown in the detailed scheme in the Supplemental Material [31]) leading to a temporal magnification of both time and spectrum. This high dispersion serves as a time-stretch system and converts between frequency and time. So, the measured intensities of both arms are $I_{1,2}^{\mathrm{measured}}(t) = I_{2,1}^{\mathrm{out}}(t/\mu)$, where μ is the magnification factor from the high dispersion fiber. With this magnification, we obtain a temporal resolution of 0.5 ps and a spectral resolution of 0.007 nm with single-shot measurements.

Another difference between our interferometer and regular SU(1,1) interferometers is the sensitivity to the phase derivative as a function of time. This is due to the Fourier transform at the second time lens. Therefore, a shift in the phase before the second time lens is mapped into a temporal shift which the interferometer detects. The generated idler as a function of time is proportional to the Fourier transform of the signal as a function of time, so there is a mapping between time in the idler arm and frequency of the signal arm, $a_2(t) = \tilde{a}_1(\omega/\xi_2)$, where $\tilde{a}_1(\omega)$ is the Fourier transform of $a_1(t)$ and ξ_2 is the mapping parameter with a dimension of $[s^{-2}]$. Let the phase change linearly as a function of time, $\varphi_{1,2} = \beta_{1,2} + \gamma_{1,2} t$. Since

$$\mathcal{F}\{\mathcal{F}\{\alpha^\dagger(t)\}^\dagger e^{i\gamma_2 \omega/\xi_2}\} = \alpha(t - \gamma_2/\xi_2), \tag{4}$$

we obtain

$$\begin{aligned} I_1^{\mathrm{out}}(t) &= |\alpha(t)|^2 G_1^2 G_2^2 + |\alpha(t - \gamma_2/\xi_2)|^2 g_1^2 g_2^2 \\ &\quad + G_1 G_2 g_1 g_2 \alpha(t) \alpha^\dagger(t - \gamma_2/\xi_2) \\ &\quad \times \mathrm{e}^{i(\varphi_1 - \beta_2)} + \mathrm{c.c.} \end{aligned} \tag{5}$$

For the idler output, we similarly define a mapping parameter ξ_1, and get

$$\begin{aligned} I_2^{\mathrm{out}}(t) &= |\tilde{\alpha}(-t)|^2 g_1^2 G_2^2 + |\tilde{\alpha}(-t - \gamma_1/\xi_1)|^2 G_1^2 g_2^2 \\ &\quad + G_1 G_2 g_1 g_2 \tilde{\alpha}^\dagger(-t) \tilde{\alpha}(-t - \gamma_1/\xi_1) \\ &\quad \times \mathrm{e}^{i(\varphi_2 - \beta_1)} + \mathrm{c.c.}, \end{aligned} \tag{6}$$

where $\tilde{\alpha} \equiv \mathcal{F}\{\alpha\}$. Therefore, by inducing a phase shift that changes linearly in time in the idler arm, we generate interference between the signal and a temporally shifted signal in the time domain. By inducing a phase shift that changes linearly in time in the signal arm, we generate interference between the spectrum of the signal and a shifted spectrum of the signal.

To verify that our time lenses are aligned, we measure the output of each time lens separately. Representative spectral measurements are shown in Figs. 2(a)–2(c), when only the first time lens operates, only the second one operates, and when both time lenses operate, respectively. An enlarged, higher-resolution spectrum of the idler is shown in

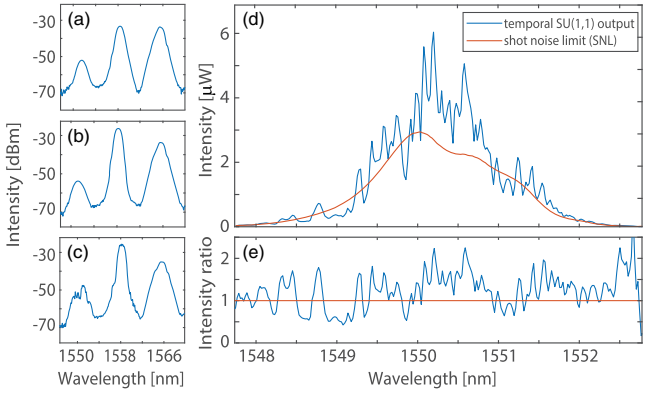

FIG. 2. Spectral measurements of the system output. (a) The output spectrum after the first time lens. The pump, signal, and idler beams are around 1558 nm, 1565 nm, and 1551 nm, respectively. (b) The output spectrum of the second time lens when the pump to the first time lens is turned off. (c) The output spectrum of the system when both time lenses are operating and interfere. (d) The blue curve denotes a high-resolution spectral measurement of the output idler. The red curve denotes the shot-noise limit which is obtained from the idler spectrum when only the first lens operates. (e) The ratio between the blue and the red curves in (d).

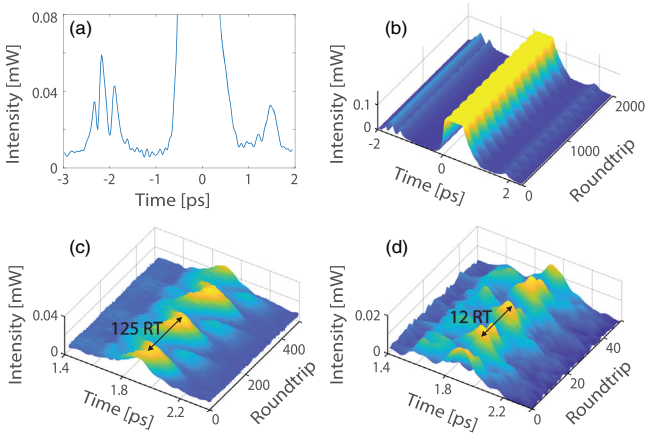

FIG. 3. (a) Representative temporal measurements of the signal, the pump, and the idler. The temporal separations between the signal or the idler and the pump are about 2 ps. (b) The measured intensity of 2000 round trips of the output as a function of time. The z axis denotes the intensity. (c),(d) An enlarged figure of the output idler wave as a function of 500 round trips showing the temporal oscillations where the EOM frequency is 4 GHz in (c), and 12 GHz in (d).

Fig. 2(d). The blue curve denotes the output of the interferometer when both time lenses operate. The red curve is the output when only the first time lens operates and is the shot-noise limit [6–8]. By comparing the output from the interferometer to the shot-noise limit in Figs. 2(d) and 2(e), we see that there are wavelengths where the intensity is weaker than the shot-noise limit. In these wavelengths, there is a destructive interference of the idler from both time lenses. This indicates that our temporal SU(1,1) is aligned and that it beats the shot-noise limit with a higher sensitivity than classical interferometers, similar to the interferometers described in Refs. [6–8].

Next, we introduce a fast-changing phase into the interferometer. We insert an electro-optic modulator (EOM) on the pump beam of the first time lens, and impose a time-changing phase on the idler. Then, we compare the output of the interferometer as a function of the EOM frequency. The duration of our time lenses is 20 ps; therefore, only for EOM frequencies of about 10 GHz we will experience a measurable phase shift within the time-lens duration. For lower EOM frequencies, we observe a regular SU(1,1) interferometer, and only for high enough EOM frequencies, we observe a temporal SU(1,1) interferometer.

We measure the output of our temporal SU(1,1) interferometer as a function of time with an oscilloscope. For every round trip of the laser, we measure the signal and idler beams and observe fringes on both of them according to the EOM phase. Representative measured results of a single round trip of the laser are shown in Fig. 3(a). We repeat the measurement over 12 000 round trips and observe an oscillating drift in the fringes. In Fig. 3(b) we show the output of 2000 round trips of the laser, where the x axis denotes the round trip, the y axis is time, and the z axis denotes the intensity. The pump, shown in the middle, at 0 ps, is saturated due to its high intensity; the signal is at -2 ps, and the idler is at 2 ps. The fringes at the idler are shifting periodically according to the phase of the EOM.

For measuring the influence of the EOM on the fringes, we repeat the previous measurement 5 times, each with a different EOM frequency, from 4 GHz up to 12 GHz. Representative results are shown in Figs. 3(c) and 3(d). The full results are presented in the Supplemental Material [31]. The results for EOM frequency of 4 GHz are shown in Fig. 3(c) and for EOM frequency of 12 GHz, in Fig. 3(d). The fringes' periodicity of the idler depends on the EOM frequency, indicating that our EOM is shifting the phase of the idler as predicted. The repetition rate of our laser is 100 MHz, so we are undersampling the oscillations of the EOM; thus, we are sampling it every time in a different cycle. Lower frequencies of the EOM will not change the phase fast enough, so we must operate in this regime. The fringes on the signal are weaker since the signal has a strong input in addition to the fringes from the time lenses while the idler is generated by the time lenses.

To demonstrate that our SU(1,1) interferometer is sensitive to the phase derivative, we evaluate the spectral correlations of the output signal and idler. In regular SU(1,1) interferometers the spectral correlation is negative; however, when our temporal SU(1,1) interferometer detects a fast-changing phase the spectral correlation changes sign.

In regular SU(1,1) interferometers, the spectral correlation is negative due to energy conservation $2\omega_p = \omega_s + \omega_i$, so if the signal frequency increases the idler frequency must decrease, and vice versa. This is also true for temporal SU(1,1) with slow-changing phase as shown by Eqs. (5) and (6) where the time parameter is positive in Eq. (5) and negative in Eq. (6). We can insert a temporal jitter $t \to t + \Delta t$, so when γ_1 and γ_2 are smaller than Δt the correlation between the timing of the peak intensity of I_1 and I_2 is negative. However, when the interferometer detects a fast-changing phase, as $\gamma_1, \gamma_2 > \Delta t$, we obtain a positive correlation. We also numerically verify this by evaluating the correlations from Eqs. (5) and (6), and obtain the calculated intensity and spectral correlations. The entire numerical derivation and code are presented in the Supplemental Material [31]. Therefore, when our temporal SU(1,1) interferometer detects fast changes in the phase, the spectral correlation changes sign.

We measure the output beams from our interferometer and evaluate the spectral correlations between the peak intensity of the signal and the idler waves. Since we are using a time-stretch system, any changes in the timing of the peak intensity are registered as spectral shifts. We measure the shift in the wavelength of the signal and the idler and show them in Figs. 4(a) and 4(b) for EOM frequencies of 4 GHz and 12 GHz, respectively. The signal is denoted by the red curve and the idler by the blue curve. We observe the negative correlation of the signal and the idler in Fig. 4(a), and the positive correlation in Fig. 4(b). We repeat this calculation to all EOM frequencies and evaluate the spectral correlation as a function of the EOM frequency, shown in Fig. 4(c). As predicted by Eqs. (5) and (6), we observe a negative spectral correlation for EOM frequencies lower than 8 GHz, and a positive correlation for higher frequencies of the EOM.

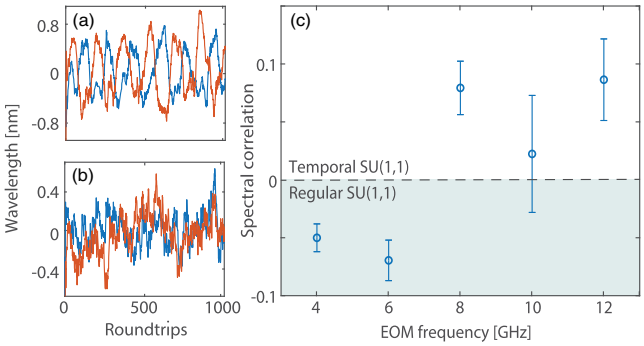

FIG. 4. (a),(b) Measurements of the wavelength shift of the signal (orange) and the idler (blue) for 4 GHz and 12 GHz frequency of the EOM, respectively. (c) Spectral correlation as a function of the frequency of the EOM, with the limit between regular and spectral SU(1,1) interferometers. The error bars are evaluated by repeating each measurement 10 times and calculating the standard deviation.

The results of the spectral correlations indicate that for lower EOM frequencies than 8 GHz, the phase is changing adiabatically compared with the resolution of our interferometer. Therefore, the temporal SU(1,1) interferometer is operating as a regular SU(1,1) interferometer with a negative spectral correlation. When the EOM frequency reaches 8 GHz its maximum phase slope is about $1/20$ rad/ps, while the temporal width of the signal that enters the HNLF is 15 ps. Therefore, the EOM phase changes significantly during the signal temporal width, leading to a positive spectral correlation.

To conclude, we developed a nonlinear temporal interferometer, able to detect ultrafast phase shifts in time by utilizing two time lenses which are situated in a $4f$ system. Our temporal interferometer has increased sensitivity, as regular SU(1,1) interferometers have, but with higher temporal resolution. It imposes interference on both temporal and spectral domains and it is sensitive to the phase derivative. We demonstrated the ultrafast detection of phase changes both in time and frequency and obtained a positive spectral correlation indicating that the interferometer is operating in the time domain. We can adopt this interferometer for studying nonclassical signals, as is done with simple time lenses [32] leading to a phase detection with high resolution of nonclassical signals. In addition, we will design an unbalanced temporal interferometer that has higher tolerances to detection losses and higher visibility than balanced interferometers [33,34]. This interferometer can be helpful for quantum imaging of ultrafast signals, temporal mode encoding, and studying the temporal structure of entangled photons.

This research was supported by the Israel Science Foundation Grant No. 2096/20, and by the Ministry of Science and Technology Grant No. 3-17812.

*mordechai.fridman@biu.ac.il

[1] M. Reck, A. Zeilinger, H. J. Bernstein, and P. Bertani, Experimental Realization of Any Discrete Unitary Operator, Phys. Rev. Lett. **73**, 58 (1994).
[2] R. Abuter, M. Accardo, A. Amorim, N. Anugu, G. Avila, N. Azouaoui, M. Benisty, J.-P. Berger, N. Blind, H. Bonnet *et al.*, First light for gravity: Phase referencing optical interferometry for the very large telescope interferometer, Astron. Astrophys. **602**, A94 (2017).
[3] B. Yurke, S. L. McCall, and J. R. Klauder, SU(2) and SU(1, 1) interferometers, Phys. Rev. A **33**, 4033 (1986).
[4] C. Brif and A. Mann, Nonclassical interferometry with intelligent light, Phys. Rev. A **54**, 4505 (1996).
[5] V. Giovannetti, S. Lloyd, and L. Maccone, Quantum-enhanced measurements: Beating the standard quantum limit, Science **306**, 1330 (2004).
[6] Y. Shaked, Y. Michael, R. Z. Vered, L. Bello, M. Rosenbluh, and A. Pe'er, Lifting the bandwidth limit of optical homodyne measurement with broadband parametric amplification, Nat. Commun. **9**, 609 (2018).

[7] L. Bello, Y. Michael, M. Rosenbluh, E. Cohen, and A. Pe'er, Broadband complex two-mode quadratures for quantum optics, Opt. Express **29**, 41282 (2021).
[8] Y. Michael, I. Jonas, L. Bello, M.-E. Meller, E. Cohen, M. Rosenbluh, and A. Pe'er, Augmenting the Sensing Performance of Entangled Photon Pairs through Asymmetry, Phys. Rev. Lett. **127**, 173603 (2021).
[9] J. L. O'brien, A. Furusawa, and J. Vučković, Photonic quantum technologies, Nat. Photonics **3**, 687 (2009).
[10] B. H. Kolner and M. Nazarathy, Temporal imaging with a time lens, Opt. Lett. **14**, 630 (1989).
[11] A. Tikan, S. Bielawski, C. Szwaj, S. Randoux, and P. Suret, Single-shot measurement of phase and amplitude by using a heterodyne time-lens system and ultrafast digital time-holography, Nat. Photonics **12**, 228 (2018).
[12] C. V. Bennett and B. H. Kolner, Principles of parametric temporal imaging. II. System performance, IEEE J. Quantum Electron. **36**, 649 (2000).
[13] H. Duadi, T. Yaron, A. Klein, S. Meir, and M. Fridman, Phase retrieval by an array of overlapping time-lenses, Opt. Lett. **44**, 799 (2019).
[14] A. Klein, I. Sibony, S. Meir, H. Duadi, M. Y. Sander, and M. Fridman, Temporal imaging with a high filling factor, APL Photonics **5**, 090801 (2020).
[15] S. Meir, A. Klein, H. Duadi, E. Cohen, and M. Fridman, Single-shot analysis of amplified correlated light, Opt. Express **30**, 1773 (2022).
[16] P. Ryczkowski, M. Närhi, C. Billet, J.-M. Merolla, G. Genty, and J. M. Dudley, Real-time full-field characterization of transient dissipative soliton dynamics in a mode-locked laser, Nat. Photonics **12**, 221 (2018).
[17] G. Herink, F. Kurtz, B. Jalali, D. R. Solli, and C. Ropers, Real-time spectral interferometry probes the internal dynamics of femtosecond soliton molecules, Science **356**, 50 (2017).
[18] A. Klein, G. Masri, H. Duadi, K. Sulimany, O. Lib, H. Steinberg, S. A. Kolpakov, and M. Fridman, Ultrafast rogue wave patterns in fiber lasers, Optica **5**, 774 (2018).
[19] A. Mahjoubfar, D. V. Churkin, S. Barland, N. Broderick, S. K. Turitsyn, and B. Jalali, Time stretch and its applications, Nat. Photonics **11**, 341 (2017).
[20] L. Lugiato, A. Gatti, and E. Brambilla, Quantum imaging, J. Opt. B **4**, S176 (2002).
[21] G. B. Lemos, V. Borish, G. D. Cole, S. Ramelow, R. Lapkiewicz, and A. Zeilinger, Quantum imaging with undetected photons, Nature (London) **512**, 409 (2014).
[22] O. S. Magaña-Loaiza and R. W. Boyd, Quantum imaging and information, Rep. Prog. Phys. **82**, 124401 (2019).
[23] V. Ansari, J. M. Donohue, B. Brecht, and C. Silberhorn, Tailoring nonlinear processes for quantum optics with pulsed temporal-mode encodings, Optica **5**, 534 (2018).
[24] T. Lettner, S. Gyger, K. D. Zeuner, L. Schweickert, S. Steinhauer, C. Reuterskiold Hedlund, S. Stroj, A. Rastelli, M. Hammar, R. Trotta *et al.*, Strain-controlled quantum dot fine structure for entangled photon generation at 1550 nm, Nano Lett. **21**, 10501 (2021).
[25] P. Guan, K. M. Roge, M. Lillieholm, M. Galili, H. Hu, T. Morioka, and L. K. Oxenlowe, Time lens-based optical Fourier transformation for all-optical signal processing of spectrally-efficient data, J. Lightwave Technol. **35**, 799 (2016).
[26] J. Azana, Time-to-frequency conversion using a single time lens, Opt. Commun. **217**, 205 (2003).
[27] C. Zhang, X. Wei, M. E. Marhic, and K. K. Wong, Ultrafast and versatile spectroscopy by temporal Fourier transform, Sci. Rep. **4**, 5351 (2014).
[28] U. Leonhardt, To invisibility and beyond, Nature (London) **471**, 292 (2011).
[29] U. Leonhardt, T. Tyc, and A. Danner, Perfect imaging with positive refraction, AIP Conf. Proc. **1291**, 22 (2010).
[30] A. Klein, I. Sibony, S. Meir, S. Shahal, H. Duadi, and M. Fridman, Overlapping time-lens array, IEEE Photonics J. **11**, 1 (2019).
[31] See Supplemental Material at http://link.aps.org/supplemental/10.1103/PhysRevLett.130.253601 for detailed experimental setup, detailed analytic derivations of all the equations in the paper, more experimental results, and numerical calculations.
[32] G. Patera, J. Shi, D. Horoshko, and M. Kolobov, Quantum temporal imaging: Application of a time lens to quantum optics, J. Opt. **19**, 054001 (2017).
[33] M. Manceau, G. Leuchs, F. Khalili, and M. Chekhova, Detection Loss Tolerant Supersensitive Phase Measurement with an SU(1,1) Interferometer, Phys. Rev. Lett. **119**, 223604 (2017).
[34] N. Huo, L. Cui, Y. Zhang, W. Zhao, X. Guo, X. Li, and Z. Y. Ou, Measurement-dependent erasure of distinguishability for the observation of interference in an unbalanced SU(1,1) interferometer, PRX Quantum **3**, 020313 (2022).